5 DC RESISTIVITY AND INDUCED POLARIZATION METHODS

ANDREW BINLEY[1] and ANDREAS KEMNA[2]

[1]*Lancaster University, Department of Environmental Science, Lancaster, LA1 4YQ, UK*

[2]*Agrosphere Institute, ICG IV, Forschungszentrum Jülich GmbH, 52425 Jülich, Germany*

5.1. Introduction and background

Dc resistivity (hereafter referred to as resistivity) and induced polarization (IP) methods allow, respectively, the determination of the spatial distribution of the low-frequency resistive and capacitive characteristics of the soil. Since both properties are affected by lithology, pore fluid chemistry, and water content (see Chapter 4 of this volume), these methods have significant potential for hydrogeophysical applications. The methods can be applied at a wide range of laboratory and field scales, and surveys may be made in arbitrary geometrical configurations (for example, on the soil surface and down boreholes). In fact, resistivity methods are one of the most widely used sets of geophysical techniques in hydrogeophysics. These surveys are relatively easy to carry out, instrumentation is inexpensive, data processing tools are widely available, and the relationships between resistivity and hydrological properties, such as porosity and moisture content, are reasonably well established. In contrast, applications of induced polarization methods in hydrogeophysics have been limited. As noted by Slater and Lesmes (2002), this is partly because of the more complex procedure for data acquisition, but also because the physicochemical interpretation of induced polarization parameters is not fully understood.

Resistivity and IP methods are deployed in a similar manner and are therefore considered jointly here. Unlike electromagnetic and radar methods, resistivity and IP require galvanic contact with the soil. Consequently, this may limit application of the methods to appropriate sites and also require longer survey times, in comparison with electromagnetic and radar techniques (although recent advances have been made in continuous survey methods, as discussed later).

Modern resistivity and IP methods have emerged from early exploration tools developed in the early 1900s. During the late 1970s, increased computing power led to the emergence of new modeling tools (for example, Dey and Morrison, 1979a,b) and the development of electrical imaging concepts (for example, Lytle and Dines, 1978), which emerged in parallel with advances in biomedical imaging. Despite the apparent complexity of present-day methodologies and algorithms, the resistivity and IP imaging tools used today are very closely related to these pioneering developments in the 1970s.

Most resistivity and IP methods still adopt the four-electrode measurement approach traditionally used in exploration geophysics. Two electrodes act as current source and sink, while the other two electrodes are used for potential difference (voltage) measurement. The emergence of imaging concepts prompted the development of multi-

electrode measurement systems in the 1980s. By the mid- to late 1990s, most instrument manufacturers were able to offer multiplexed instruments, and in some cases multi-measurement channel hardware, thus enabling reduced survey time. For hydrogeophysical applications, this also meant the ability to study time-dependent processes.

Modern resistivity and IP methods both have powerful imaging capability. Terms such as electrical resistance (or resistivity) tomography (ERT), electrical impedance tomography (EIT), and applied potential tomography (APT) have been widely used in geophysics, biomedicine, and process engineering to describe imaging of electrical properties. In geophysics, the term "tomography" was originally used for investigations in which sensors bounded the region under investigation. Eventually, the term became synonymous with any form of imaging, even using linear arrays of sensors, as in surface deployed surveys. As imaging techniques have developed to study 3D and even 4D systems, the term "tomography" is not appropriate, and we prefer here to simply use the term "imaging".

Conventional dc resistivity and IP methods for geophysical exploration are covered well in many texts, for example Telford et al. (1990) and Reynolds (1998). However, these texts, and others, do not address more advanced developments of these methods (for example, cross-borehole imaging) or approaches for small-scale characterization (related to those used in the biomedical or process engineering fields). All of these approaches now provide the hydrogeophysicist with more flexible investigative tools. Our aim here is to review a wide range of resistivity and IP tools available for hydrogeophysical investigation. In Section 5.2, we outline the basic measurement principles for these methods. This is followed, in Section 5.3, by a presentation of the range of survey configurations. Data processing is required to transform measured data to a 1D, 2D, or 3D spatial distribution of electrical properties and details of the methods commonly used are covered in Section 5.4. In Section 5.5, we discuss important practical issues that must be addressed before the techniques covered here can be applied. Finally, in Section 5.6, we summarize future challenges for developers and users of resistivity and IP methods for hydrogeophysical surveys.

5.2. Basic measurement principles

5.2.1 RESISTIVITY

In the resistivity method, the spatial variation of resistivity ρ (or conductivity σ, the inverse) in the field is determined using four-electrode measurements. Two (transmitter) electrodes are deployed to create an electrical circuit. Measurement of the potential difference (voltage) between the two other electrodes permits determination of an apparent resistivity (i.e., the resistivity a homogenous halfspace should have to give the actual measurement). Inverse methods may be applied to such measurements to determine an image of the subsurface structure, as illustrated later. Electrodes may be placed on the ground surface and/or in boreholes.

Stainless steel is the most widely used electrode material for field measurements, although others, such as copper or brass, are also used. To avoid polarization at the electrodes, an alternating power source is utilized. A switched square wave (see Figure 5.1) is the most common current wave form; it is generally applied at frequencies of about 0.5 to 2 Hz. As shown in Figure 5.1, a background (self-potential) voltage, V_{sp}, may be observed. Note that the level of this may change over time, but such drift is easily removed owing to the shape of the injected waveform. The measured transfer resistance is given by $R = V_p / I$, where V_p is the primary (peak) voltage and I is the injected current, as shown in Figure 5.1. Note that the voltage series in Figure 5.1 is idealized since no capacitive (electrical charge storage) effects are observed. In practice, such effects will exist, as outlined in Section 5.2.2.

For a 3D, isotropic electrical conductivity distribution, $\sigma(\mathbf{r})$, the electric potential, $V(\mathbf{r})$, at a point $\mathbf{r}$ due to a single current electrode, idealized as a point source at the origin with strength I, is defined by the Poisson equation

$$\nabla \cdot (\sigma \nabla V) = -I\delta(\mathbf{r}), \tag{5.1}$$

subject to the condition

$$\frac{\partial V}{\partial n} = 0 \tag{5.2a}$$

at the ground surface and the condition

$$V = 0 \tag{5.2b}$$

at the other, infinite boundaries. Here, δ is the Dirac delta function and n is the outward normal.

As illustrated in Figure 5.2, current flow in a homogenous earth from an electrode placed on the ground surface will follow

$$V = \frac{\rho I}{2\pi}\frac{1}{r}, \tag{5.3}$$

where ρ is the resistivity, and r is the distance from the electrode. Since the apparent resistivity, ρ_a, is defined as the resistivity of a homogenous earth to which the measured transfer resistance is equivalent, the above equation may be used with the principle of superposition to derive expressions for the apparent resistivity of specific electrode arrangements.

A number of electrode configurations are commonly used for ground-surface surveys. Figure 5.3 illustrates the Wenner, dipole-dipole, and Schlumberger surveys. Others (for example, pole-pole, pole-dipole) are also deployed (see, for example, Telford et al., 1990). As an example, for the Wenner array, the apparent resistivity, ρ_a, is given by

$$\rho_a = 2\pi a R, \tag{5.4}$$

where a is electrode spacing (as shown in Figure 5.3).

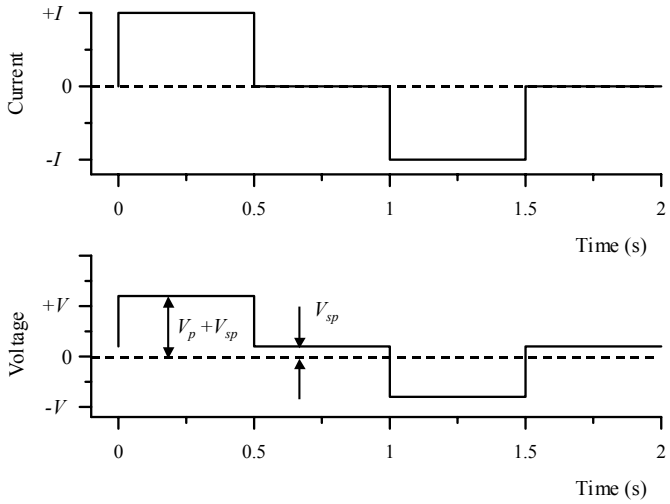

Figure 5.1. Typical current and idealized voltage waveforms for field dc resistivity surveys. V_p is the primary voltage, V_{sp} is the observed self potential voltage.

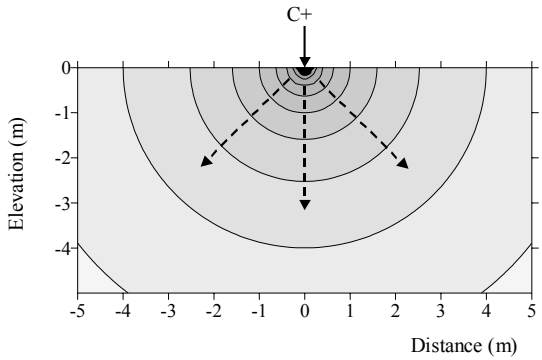

Figure 5.2. Potential variation in a half space with uniform resistivity distribution due to current injection at the ground surface

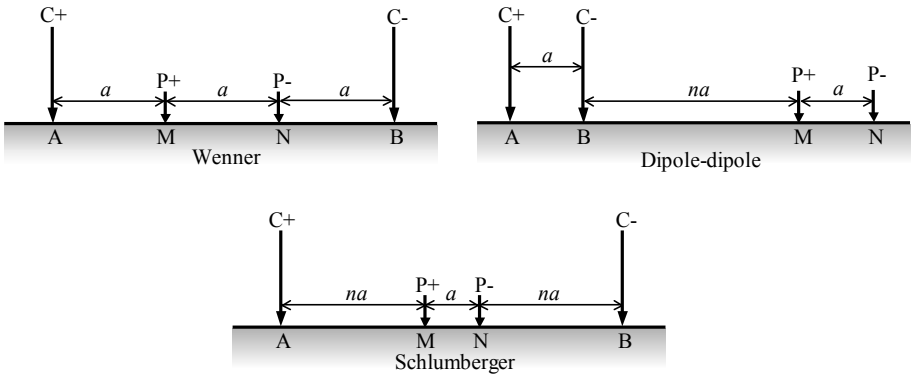

Figure 5.3. Example surface electrode configurations

5.2.2 INDUCED POLARIZATION

Whereas the resistivity of the soil is principally controlled by electrical conduction within the pore fluid, IP is strongly affected by processes at the fluid-grain interface (see Chapter 4 of this volume). In an IP survey, both the resistive and capacitive properties of the soil are measured. As a result, IP surveys, at least in theory, permit additional information about the spatial variation in lithology and grain-surface chemistry to be determined.

IP measurements are made in the field using a four-electrode arrangement. Measurements can be made in time-domain or frequency-domain mode. For the former, the voltage decay with time is measured after the current injection is stopped (see Figure 5.4). The gradual (rather than abrupt) decrease in measured voltage is a complex function of the electrical charge polarization at the fluid-grain interface, and the conduction within the pore fluid and along the grain boundaries.

Seigel (1959) defined the apparent chargeability as

$$m_a = \frac{V_s}{V_p}, \tag{5.5}$$

where V_s is the secondary voltage (voltage immediately after the current is shut off) and V_p is the primary voltage. The secondary voltage is difficult to measure accurately in the field and, as a result, an integral measure of apparent chargeability,

$$M_a = \frac{1}{(t_2 - t_1)} \frac{1}{V_p} \int_{t_1}^{t_2} V(t)dt, \tag{5.6}$$

is used, as illustrated in Figure 5.4. Units of chargeability are typically millivolts per volt (mV/V).

In frequency-domain mode, a phase-shifted voltage relative to an injected alternating current is measured. Traditionally, the percent frequency effect (PFE) has been used as an IP measure in the frequency-domain. Here, a comparison of impedance magnitudes is made at different injection frequencies (see for example, Reynolds, 1998). Alternatively, the impedance (in terms of magnitude and phase angle) may be used as a measure of IP. This is commonly referred to as complex resistivity. By applying the injected current at different injection frequencies, a spectrum of impedances results. This is commonly referred to as spectral IP (SIP).

Whereas traditional IP time-domain instruments measured a number of points on a decay curve, modern instruments digitize the signal at relatively high sampling rates and permit Fourier analysis in the frequency-domain. In doing so, time-domain instruments can also provide a measure of IP in terms of complex resistivity, although the frequency range will be constrained by the sampling rate of the instrument.

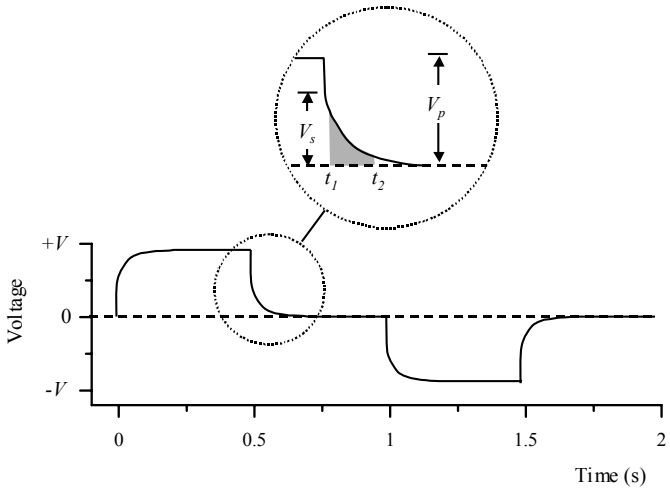

Figure 5.4. Measurement of time-domain induced polarization

IP can be measured in the field using a similar approach to that for dc resistivity. The potential electrodes should, ideally, be nonpolarizing (for example, copper-copper sulfate), although conventional dc resistivity electrodes have been used with some success (see Dahlin et al., 2002). To avoid electromagnetic coupling effects, the cable used for current injection should be short and isolated, as much as possible, from cables connected to the potential electrodes. Dipole-dipole arrays for ground-surface surveys are often preferred because of their minimal coupling effects and safer operating conditions (particularly for long survey transects). For IP surveys, injection currents often need to be much higher than those used for dc resistivity to ensure good signal-to-noise ratios. This is particularly important when using a dipole-dipole electrode configuration.

There are clearly a number of measures of IP. The measured apparent chargeability will depend upon the time window (t_1 to t_2) used, PFE will depend upon the two selected injection frequencies, and the phase angle of the impedance will depend upon the injection frequency. Furthermore, all of these measured properties will be a function of the pore fluid conductivity and the grain-surface polarization. Slater and Lesmes (2002) demonstrate how these measurements may be scaled to derive IP parameters that are dependent only on polarization at the grain-surface. In doing so, an IP survey can be used to provide information about the conductivity of the pore space (i.e., fluid chemistry and/or pore water content), as in a conventional resistivity survey, together with information about the grain-surface chemistry (lithology). Slater and Lesmes (2002) illustrate this approach using two field studies, showing how zones of high and low clay content may be delineated irrespective of pore fluid chemistry. Kemna et al. (2004a) show further evidence of the value of such an approach, in this case through cross-borehole IP imaging.

5.3. Survey configurations

Electrical methods may be applied in a range of survey configurations. The approach adopted will depend on: (1) the objectives of the survey, (2) the expected spatial variability of electrical properties, (3) access to suitable electrode sites, (4) equipment availability, and (5) data processing capabilities. Resistivity and IP methods are commonly applied on the ground surface using multiple four-electrode sites. This allows a reasonably low-cost way of mapping lateral and vertical variability in resistivity. Deployment of electrodes in boreholes will permit improved resolution at depth and, relatively recently, borehole-to-borehole or cross-borehole methods have been developed for this purpose. We list here the main configuration types and summarize the strengths and weaknesses for each when applied for hydrogeophysical investigations. In some cases, significant postprocessing of data (using modeling techniques discussed below) is required. In others, minimal effort is required to achieve the survey objectives. The survey configurations discussed apply to both resistivity and IP methods.

5.3.1 SURFACE PROFILING

The term "profiling" is used here to describe surveys of the lateral variability (i.e., at a constant depth) of electrical properties. Profiling is typically carried out along ground-surface transects. Using a particular electrode array (Wenner, dipole-dipole, etc. [see Figure 5.3]), measurements are made at different positions while keeping the electrode spacing constant. Each four-electrode position will provide an integrated measure of the electrical property. The spatial variability of signal contribution will depend on the array type (see for example, Barker, 1979) and the (unknown) variability of the resistivity. Typically, a single position is designated for the measurement at one four-electrode site. The lateral position will be the center of the four-electrode array; the depth position will depend on the configuration and spacing. For example, using a Wenner array, half the electrode spacing ($a/2$) is often assigned as the approximate depth zone of influence.

Profiling is useful for relatively rapid spatial coverage and does not require specialized multicore cables, multiplexing units, or lengthy setting out. The method is routinely used by archeological geophysicists for single depth surveys over large areas, often using a twin-array (mobile pole-pole) configuration (see for example, Mussett and Khan, 2000). Equipment to permit continuous profiling has been developed in Denmark (Sørensen, 1996) allowing surveys of 10 km in one day by taking 1 m spaced measurements using a string of electrodes towed by a vehicle. Hydrogeophysical uses of such surveys may include near-surface soil moisture, salinity, or textural mapping. However, because profiling does not provide information about variability with depth, electromagnetic methods may be preferred owing to their improved survey speed. By using large electrode spacing, deeper investigations may allow mapping of vertical hydrogeological boundaries or fracture zones (for example, Bernard and Valla, 1991).

5.3.2 VERTICAL ELECTRICAL SOUNDING

A vertical electrical sounding (VES) is used to determine the variation of electrical properties with depth at a single location in space, assuming no lateral variation. Four-electrode measurements are made with progressively larger spacing, centered at the same position. This provides a sounding curve as shown in Figure 5.5, which may be interpreted, using methods described below, to delineate horizontal layers. Such an approach has been used widely to differentiate hydrogeological units and, in some cases, estimate hydrological properties (e.g., Kosinski and Kelly, 1981; Börner et al., 1996). It has also been adopted in a number of studies of dynamic hydrological processes (e.g., Kean et al., 1987; Frohlich and Parke, 1989) and to estimate travel times of pollutants moving through the vadose zone (Kalinski et al., 1993).

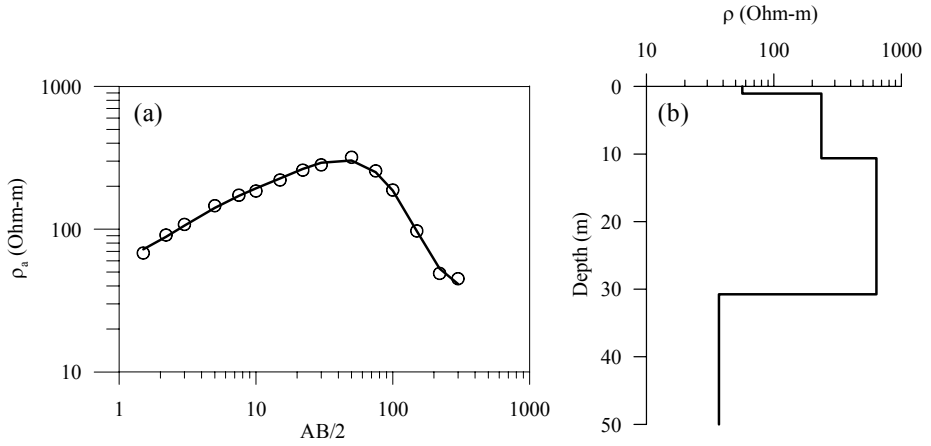

Figure 5.5. (a) Example of a Schlumberger array sounding curve from VES survey. Circles indicate measured data and solid line shows modeled curve. AB/2 (in m) is the half distance between the current electrodes (see Figure 5.3).
(b) Interpreted model of resistivity as a function of depth at a single location.
(Data and inversion available at www.geol.msu.ru/deps/geophys/rec_labe.htm)

The VES method suffers from the necessary, but often unrealistic, assumption that 1D variations in electrical properties exist. Most modern dc resistivity and IP instruments offer the capability of addressing electrodes using multicore cables. When using such an arrangement, information about the lateral variability of electrical properties can be easily determined using combined sounding and profiling (see Section 5.3.4). VES surveys are only advantageous when such multiplexing of electrode configurations is not available. Simms and Morgan (1992) illustrate how VES survey interpretation can be ambiguous or non-unique.

5.3.3 AZIMUTHAL SURVEYS

Azimuthal surveys are conducted by carrying out four-electrode measurements at different horizontal angles, centered on a single point. This provides information about the azimuthal anisotropy of the electrical property. Such surveys can be useful for

determining the orientation of fracture planes (see for example, Taylor and Fleming, 1988).

5.3.4 SURFACE IMAGING

Surface imaging combines surface profiling and vertical sounding to produce a 2D or 3D image of the subsurface resistivity or IP properties. Although the method has been widely used for decades, the relatively recent development of computer controlled dc resistivity and IP instruments, coupled with advances in modeling techniques, have led to a widespread use of this approach for hydrogeological applications.

A surface imaging survey is carried out by acquiring profiles along transects using different electrode spacings. 3D surveys may be carried out as a sequence of 2D surveys in parallel to each other (for example, Dahlin and Loke, 1997) or as a true 3D survey using a 2D grid of electrodes on the ground surface (see for example, Loke and Barker, 1996). A pseudo-section of electrical properties is normally constructed: for each measurement, a survey level and lateral position (midpoint of the four electrodes) is determined, and the apparent resistivity assigned to that position. Figure 5.6 illustrates the concept of building up the pseudo-section for a 2D survey using a Wenner electrode configuration. Here, each survey level corresponds to a different electrode spacing. As the spacing increases, the effective depth of sensitivity increases. Note, however, that the pseudo-section does not necessarily show an accurate image of the subsurface distribution of resistivity, it merely serves as a means of plotting measured data. In Figure 5.7 pseudo-sections are shown for Wenner and dipole-dipole configurations, for a synthetic model (shown in Figure 5.7a). Note that the two configurations yield a different response, since a pseudo-section is not a true vertical cross section. This figure also reveals that each configuration type has different signal sensitivity patterns: Wenner pseudo-sections will tend to exaggerate lateral layering, whereas dipole-dipole surveys will reveal better vertical features.

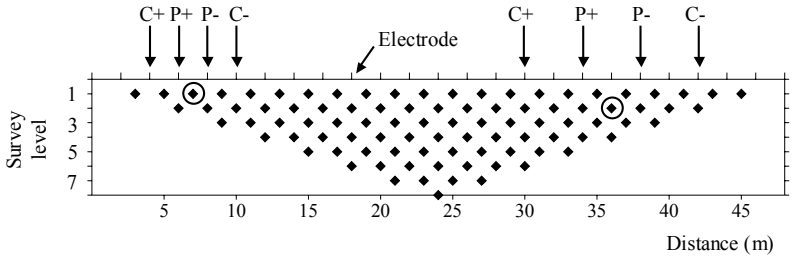

Figure 5.6. Surface electrical imaging: building a pseudo-section. Circles identify the location assignment for the two measurement configurations shown. Each survey level corresponds to a different electrode spacing.

Modeling of electrical imaging data, using methods described in Section 5.4, can provide an image of modeled resistivity within the zone of investigation. Figure 5.8 illustrates this for the synthetic model example in Figure 5.7. The modeled sections show greater similarity to the model itself than the pseudo-sections; however, note again that the Wenner model tends to reveal the horizontal element of the target,

whereas the vertical structure is better resolved using the dipole-dipole model. Note also that the modeling process does not recover the true structure of the target. This is partly due to the variation in signal sensitivity within the region (particularly towards the edges) but also due to the smoothing of the model inversion process (as discussed below).

Numerous examples of surface electrical imaging applied to hydrogeological problems exist, a number of which are discussed in Chapter 14 of this volume. The method is now widely used for shallow investigations (for example, to depths of 30 m). An entire survey along a transect 100 to 200 m long, covering depths to 20 to 30 m, can be carried out in under two hours using multicore cables and computer-controlled instrumentation. Longer surveys, whilst maintaining the same depth of survey, can be achieved using "roll along" extensions—see for example, Dahlin (1993). Panissod et al. (1997) and Christensen and Sørensen (2001) both describe methods for continuous electrical soundings using vehicle-towed electrode arrays.

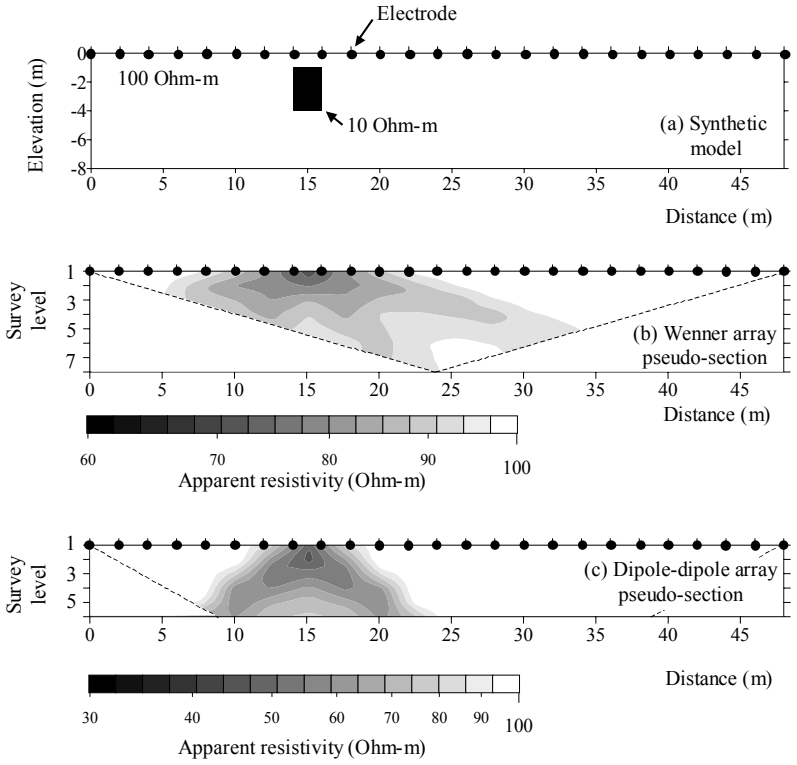

Figure 5.7. Surface electrical imaging example pseudo-sections: (a) synthetic model, (b) Wenner pseudo-section, (c) dipole-dipole pseudo-section

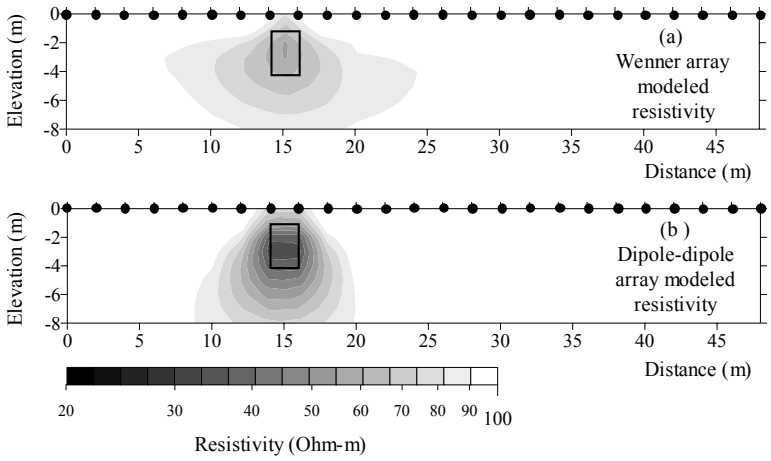

Figure 5.8. Modeled resistivity sections for the synthetic model in Figure 5.7 (inversion tools available at http://www.es.lancs.ac.uk/es/people/teach/amb)

5.3.5 SINGLE BOREHOLE SURVEYS

Electrical surveys can be conducted in several modes using electrodes deployed in a borehole. Electrodes may be permanently installed in a borehole, using suitable backfill material (ideally the native material, i.e. drill returns) in the vadose zone. In the saturated zone, open (uncased) boreholes can be used as electrode sites and, relatively recently, arrays have been manufactured for this purpose, some with isolation packers to minimize current flow along the borehole water column. Slotted plastic cased wells may also be used as electrode sites below the water table, although the well screen will add to the resistance between electrode and host material, and channeling along the borehole water column will occur unless isolation packers are used. In theory, however, the effect of the channeling can be accounted for in any data modeling by incorporating measurements of borehole water electrical conductivity and borehole geometry.

A common borehole-based approach used in mineral exploration is the mise-à-la-masse method. In such a survey, one of the current carrying electrodes is installed in a borehole at depth, while the other current electrode is installed on the surface at a significant distance from the borehole. Potential measurements are then made at several sites on the surface, relative to a remote potential electrode, as shown in Figure 5.9. The measurements may be compared to modeled voltages for a homogenous resistivity. In mineral exploration, such measurements can help delineate electrically conductive ore bodies. In hydrological studies, the method may be used to identify orientation of fracture planes or the migration of an electrically conductive tracer injected in the well used for current injection (see for example, Osiensky, 1997). Improved characterization may be achieved by supplementing the ground-surface measurements with electrodes installed in other boreholes (for example, Nimmer and Osiensky, 2001). In all cases, interpretation may be subjective unless modeling techniques are used (see for example, Bevc and Morrison, 1991).

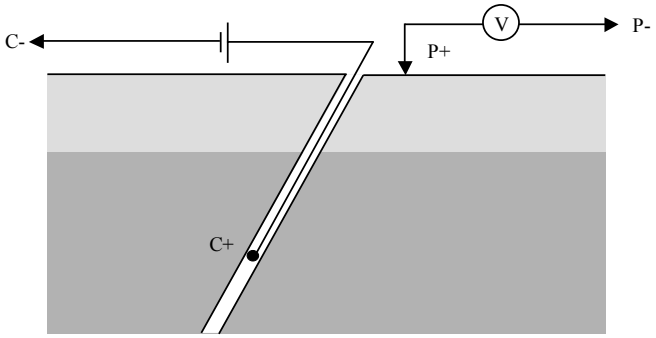

Figure 5.9. Mise-à-la-masse survey layout

Arrays of electrodes in a borehole can be used to obtain profiles in the same manner as a surface electrical profile. Such an approach provides greater support volume of measurements than conventional borehole-water electrical conductivity sampling. These methods also offer improved sensitivity to variation in electrical properties with depth in comparison with surface-applied electrical surveys. Binley et al. (2002a), for example, used a 32-electrode array installed in the vadose zone of a sandstone aquifer to assess changes in moisture content in unsaturated sandstone over a two-year period and detected changes in resistivity associated with a 2 % absolute variation in moisture content (see also Chapter 14 of this volume).

Imaging using a borehole electrode array is a straightforward extension of surface electrical imaging, although applications have been rare. These surveys may be supplemented with surface electrodes to form a similar geometrical arrangement to vertical seismic profiling (see Chapter 8 of this volume); however, for electrical surveys, the signal sensitivity will be confined to areas close to the borehole and surface electrode sites.

5.3.6 CROSS-BOREHOLE SURVEYS

Cross-borehole electrical resistivity surveying is an extension of conventional surface resistivity imaging. Using measurements from electrodes placed in at least two boreholes, sometimes supplemented by surface electrodes, an image of the resistivity between the boreholes is obtained. One of the earliest attempts to use such an arrangement is outlined by Daily and Owen (1991). Daily et al. (1992) demonstrated how this technique can be applied in hydrogeophysics, in their study of monitoring moisture movement in the vadose zone. Following the development of robust inversion routines and suitable data acquisition systems, cross-borehole resistivity has been applied to a wide range of hydrogeophysical problems, including vadose zone studies (Binley et al., 2002b; French et al., 2002), characterizing the transport of tracers in the subsurface (Slater et al., 2000; Kemna et al., 2002), monitoring remediation technologies (Ramirez et al., 1993; Schima et al., 1996) and monitoring leakage from underground storage tanks (Ramirez et al., 1996). A case study illustrating the use of

cross-borehole resistivity imaging to monitor vadose zone flow is described in Chapter 14 of this volume.

The main advantages of cross-borehole imaging compared to surface imaging, are that: (1) high resolution at depth is possible and (2) investigations can be made without the need for surface access (for example, surveys under buildings are possible). The disadvantages are that: (1) boreholes are required, (2) data sensitivity is constrained to the region between the boreholes, (3) data acquisition may require more sophisticated instrumentation, (4) for vadose zone surveys, noise levels may be much higher than those using surface electrodes, owing to weaker electrical contact (increased contact resistance), and (5) data processing is more complex.

Using borehole-deployed electrodes, a very large number of measurement schemes are possible. In Figure 5.10, two example bipole-bipole schemes are shown (here we use the term bipole-bipole to differentiate from the conventional surface dipole-dipole array). Other arrangements using remote (pole) electrodes are also possible. In the AM-BN scheme shown in Figure 5.10a, current is injected between the two boreholes and a potential difference is measured between the boreholes. In the AB-MN scheme in Figure 5.10b, current is injected between electrodes in the same borehole, and the potential difference is measured between electrodes in the other borehole. The AM-BN scheme has good signal-to-noise characteristics, in comparison to AB-MN, because of the dipole length. Bing and Greenhalgh (2000) have studied these schemes, and others, in a synthetic modeling exercise, and demonstrate the impact of poor signal-to-noise characteristics on resistivity images.

Although such synthetic studies are useful, the concept of a "universal" measurement scheme for cross-borehole imaging is probably not achievable. Conditions for cross-borehole surveys are extremely variable because of: (1) contrasts in electrode contact and influence of backfill or any borehole water column, (2) different borehole separations, and (3) instrumentation resolution and measurement rate. Moreover, the assessment of the true measurement errors must be considered in any analysis of cross-borehole electrical measurements, because such errors will be strongly dependent on the environment to which the method is applied. It is thus extremely useful to consider the acquisition geometry of cross-borehole methods on a case-by-case basis.

To illustrate the resolution of cross-borehole resistivity imaging, Figure 5.11 shows an example of a synthetic model and the associated resistivity distribution. For this example, the AB-MN scheme with an electrode spacing of 8 m was used. The "target" is well resolved, but the final image is smoothed, owing to the inverse modeling scheme adopted. In Figure 5.12, the effect of increased borehole spacing is shown. Here, the final image reveals a more smeared effect caused by the reduced sensitivity towards the center of the image. Clearly, care should be taken to design the position of borehole arrays when using cross-borehole techniques. This is discussed further in Section 5.5.

Schenkel (1995) has demonstrated how steel-cased boreholes can be used to determine electrical resistivity images between boreholes. This approach is no different from the conventional cross-borehole arrangement, except that the highly conductive well casing

is accounted for in the model analysis. Although such an approach has reduced sensitivity, given the widespread availability of existing steel cased wells, this method offers potential for further development.

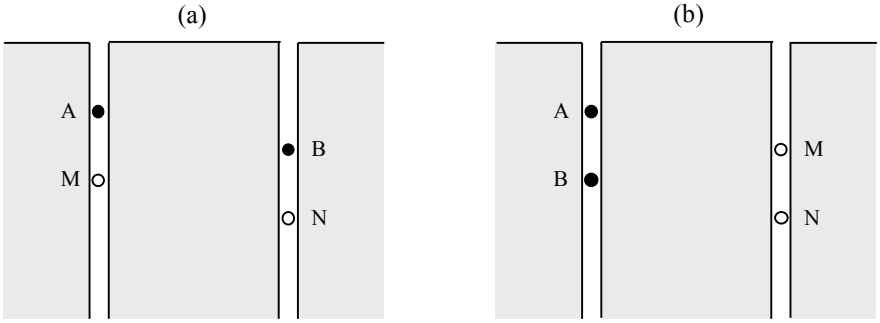

Figure 5.10. Example measurement configuration for cross-borehole resistivity imaging. Electrodes A and B are for current injection, M and N are for voltage measurement. Scheme (a) is AM-BN and scheme (b) is AB-MN.

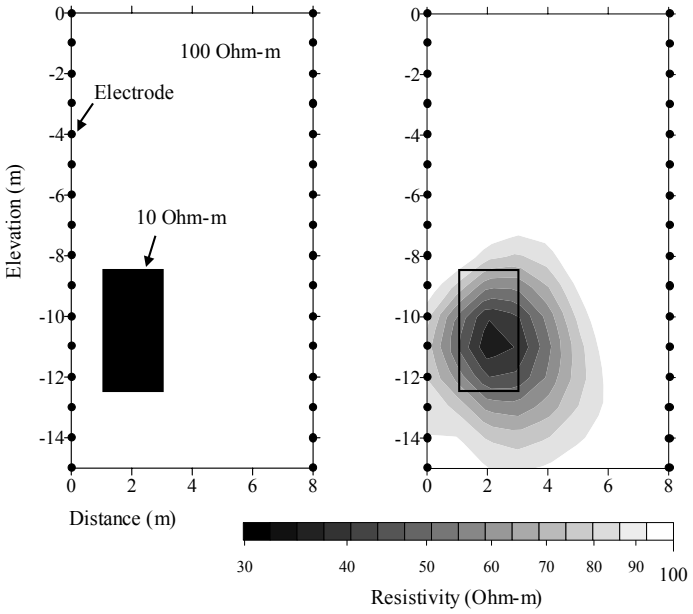

Figure 5.11. Cross-borehole resistivity imaging applied to a synthetic model

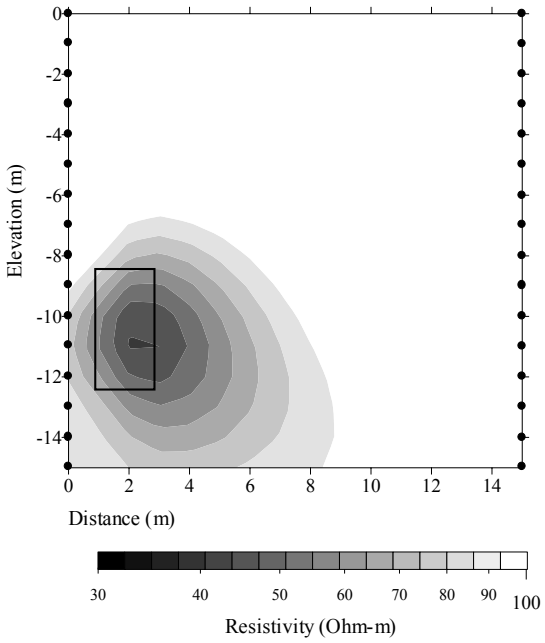

Figure 5.12. Cross-borehole resistivity imaging applied to a synthetic model to illustrate reduced resolution with increased borehole spacing. The 10 ohm-m target outline is indicated in the image. The background resistivity of the model is 100 ohm-m, as in Figure 5.11.

5.3.7 CORE AND BLOCK SCALE IMAGING

Electrical methods have also been applied to image the variability of electrical properties at the core or block scale. In fact, one of the early applications of electrical imaging was the study of rock cores by Daily et al. (1987) using circular electrode arrays. Binley et al. (1996) also used circular arrays in their investigation of preferential flow in 0.3 m diameter undisturbed soil cores, and Ramirez and Daily (2001) demonstrate how electrical imaging can be used to study changes in moisture distribution in a 3 m × 3 m × 4.5 m block of welded tuff. Because the electric potential field can be modeled for any arbitrary geometry, there are no constraints on the size and shape of the object under investigation. In Chapter 15 of this volume, examples of core-scale imaging for hydrogeophysical studies are shown.

5.4. Modeling and data inversion

5.4.1 GENERAL CONCEPTS

The ultimate goal of electrical methods is to derive the distribution of (low-frequency) electrical properties inside an object, here generally the subsurface, from a set of measurements conducted on the boundary of the object, or at least outside the region of interest, according to the principles outlined in the previous section. The theoretical

outcome of such a measurement can be mathematically determined (modeled) for given electrical properties from the governing physical law, the Poisson equation, subject to given boundary conditions (Equations (5.1) and (5.2)). This exercise defines the so-called "forward problem". For the purpose of subsurface investigations, however, the "inverse problem" needs to be solved, i.e., given a set of measurements (data), the distribution of electrical properties (model) is sought that explains the observations to an acceptable degree (Figure 5.13). For resistivity surveys, data will be in the form of transfer resistances or apparent resistivities, and the model will be parameterized in terms of resistivity or conductivity. For IP surveys, data will be in the form of apparent chargeability or transfer impedance, and the model will be parameterized in terms of intrinsic chargeability or complex resistivity, respectively.

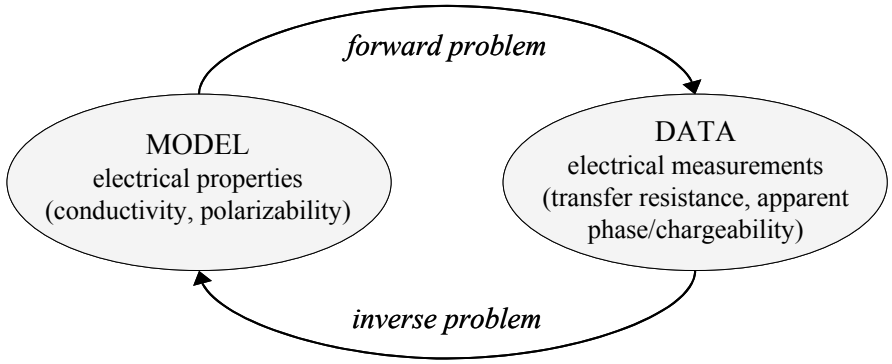

Figure 5.13. Definition of electrical forward and inverse problem

Unfortunately, there is no unique solution to this problem (this has promoted development of stochastic approaches such as those discussed in Chapter 17 of this volume). Electrical methods bear a certain degree of inherent non-uniqueness, i.e., there typically exists a variety of different models that effectively produce the same response. In addition, because of practical limitations, data are neither complete nor perfectly accurate, but mostly insufficient and inconsistent. Therefore, in principle, an infinite number of models fit the data within a given level of uncertainty. However, by systematically restricting the model search in the inversion process, for instance by claiming predefined model characteristics, a "unique" solution with practical relevance can be obtained. This is usually accomplished by formulating the inverse problem as a regularized optimization problem, which involves minimization of an objective function comprising both data misfit (measured vs. modeled) and a penalty term accounting for deviations from the desired model attributes.

Starting with the formulation of the electrical forward problem, the following discussion focuses on the principles of appropriate inversion strategies. Moreover, different approaches for appraisal of the final inversion result are addressed; these are essential tools for a critical interpretation in real applications. We include details of the approaches here, since this material is not covered in existing exploration geophysical texts. The reader who is not concerned with details of the modeling approaches may

wish to omit the following and go directly to Section 5.5. It is, however, useful for any user of resistivity and IP methods to be aware of the limitations and assumptions of the modeling tools used for data processing. Inverse models provide an image of electrical properties, but the image is subject to uncertainty. All data will be subject to error, and the user should be aware of these errors in order to prevent overfitting of any inverse model. The model itself will be an approximation and thus acts as another source of error. Data sensitivity will vary considerably in the image and an appreciation of how to explore such variability will allow greater confidence in assessing the reliability of the image values. Many inverse methods for resistivity and IP methods employ some form of smoothing to ensure that a solution is reached. In some cases, such smoothing may be inappropriate—for example, if it is known that sharp contrasts exist, perhaps resulting from lithological boundaries.

5.4.2 FORWARD PROBLEM

5.4.2.1 DC Resistivity

If the conductivity distribution is 2D, for instance constant in the y direction, application of the Fourier transform

$$\widetilde{V}(x,k,z) = \int_0^\infty V(x,y,z)\cos(ky)\,\mathrm{d}y \tag{5.7}$$

to Equation (5.1) yields a simplified, 2D problem (for example, Hohmann, 1988), that is,

$$\frac{\partial}{\partial x}\left(\sigma\frac{\partial\widetilde{V}}{\partial x}\right)+\frac{\partial}{\partial z}\left(\sigma\frac{\partial\widetilde{V}}{\partial z}\right)-k^2\sigma\widetilde{V}=-\frac{I}{2}\delta(x)\delta(z)\,, \tag{5.8}$$

with k being the wavenumber. Once this differential equation is solved for the transformed potential $\widetilde{V}(x,k,z)$, an inverse Fourier transform must be applied to obtain $V(\mathbf{r})$ (for example, LaBrecque et al., 1996; Kemna, 2000).

For a horizontally layered earth model, i.e., σ only varying with z, a compact solution of the Poisson equation can still be formulated. Assuming for instance a Schlumberger electrode configuration (see Figure 5.3), which is typically adopted for vertical electrical soundings (see Section 5.3.2), the apparent resistivity is given by the so-called Stefanescu integral (for example, Koefoed, 1979):

$$\rho_\mathrm{a}(r) = r^2\int_0^\infty T(\lambda)J_1(\lambda r)\,\lambda\,\mathrm{d}\lambda\,, \tag{5.9}$$

where r is the half distance between the current electrodes, J_1 is the Bessel function of order one, and the kernel $T(\lambda)$ is a function of the given layer thicknesses and resistivities, with λ being an integration variable (wavenumber).

Whereas the integral in Equation (5.9) can be readily calculated, for instance using fast filtering techniques (for example, Anderson, 1979; Christensen, 1990), for arbitrary 2D or 3D conductivity distributions, computationally more expensive numerical approaches are required to solve Equation (5.8) or (5.1). In these cases, finite element

(FE) or finite difference (FD) methods are typically used, where the continuous conductivity distribution is approximated by a mesh of individual elements or cells, each with constant conductivity. The potential is then calculated at discrete points (nodes of the mesh) by solving a linear system of equations derived from the discretized differential equation and boundary conditions. Hohmann (1988) provides an overview of the approach. Details on the use of FE and FD methods to solve the dc electrical problem are well documented in the literature (for example, Coggon, 1971; Dey and Morrison, 1979a,b; Pridmore et al., 1981; Lowry et al., 1989; Spitzer, 1995; Bing and Greenhalgh, 2001). A direct comparison of the performance of both methods was recently presented by Li and Spitzer (2002). However, in general, FE methods are preferred if greater flexibility with respect to mesh geometry is desired, for instance to account for irregular electrode positions or to incorporate topography.

5.4.2.2 Induced Polarization

Two different approaches are commonly used to model IP data. According to Seigel (1959), the time-domain voltage response of a polarizable medium with conductivity σ_{dc} and intrinsic chargeability m can be interpreted as the response of a nonpolarizable medium with decreased conductivity $\sigma_{ip} = (1-m)\sigma_{dc}$. This results from the fact that any present polarization dipoles effectively reduce the overall current density. Consequently, the apparent chargeability m_a (see Equation (5.5)) can be modeled by carrying out dc resistivity forward models for σ_{ip} and σ_{dc}, according to (for example, Oldenburg and Li, 1994)

$$m_a = \frac{f[(1-m)\sigma_{dc}] - f[\sigma_{dc}]}{f[(1-m)\sigma_{dc}]}. \tag{5.10}$$

In Equation (5.10), f represents the forward modeling operator implicitly defined by the equations stated in the previous paragraph for 1D, 2D, and 3D conductivity distributions, respectively. An alternative, frequency-domain approach is based on the combined description of conduction and polarization properties by means of a complex conductivity, σ^*. In the quasi-static frequency limit (typically < 10 Hz), a complex-valued Poisson equation,

$$\nabla \cdot (\sigma^* \nabla V^*) = -I\delta(\mathbf{r}), \tag{5.11}$$

may be solved for a complex potential, V^*, analogous to the dc case outlined above. From V^*, both magnitude and phase, as the relevant dc resistivity and IP data, are obtained. Weller et al. (1996), for example, followed this approach using a finite-difference framework.

5.4.3 INVERSE PROBLEM

To formulate the inverse problem, the considered distribution of electrical properties is discretized into a set of parameters defining a model vector **m**. While for 1D problems, **m** normally contains the conductivities and thicknesses of a multilayer model, for arbitrary 2D and 3D distributions its elements generally correspond to the conductivities of the individual elements or cells (or lumped blocks thereof) of the FE or FD mesh used in the forward modeling. That is,

$$m_j = \ln \sigma_j \quad (j = 1, ..., M). \tag{5.12}$$

Here, the logarithm accounts for the large possible range in earth conductivity. Analogously, the given set of measured transfer resistances, R_i, is assembled in a data vector **d** according to

$$d_i = -\ln R_i \quad (i = 1, ..., N). \tag{5.13}$$

Again log-transformed data are normally used on account of the wide range in observed resistances for arbitrary electrode configurations, while the minus sign in Equation (5.13) accounts for a physical dimension consistent with Equation (5.12).

The inverse problem now is to find a model **m** which, using the forward mapping according to the above equations, (5.1), (5.8), or (5.9), reproduces the data **d** to the specified level of uncertainty. However, since inherent non-uniqueness of the resistivity inverse problem, together with the presence of data errors, can effectively lead to an extremely ill-posed numerical problem, additional constraints must be imposed on the inversion. This is normally accomplished by solving the inverse problem as a regularized optimization problem (Tikhonov and Arsenin, 1977), where an objective function of the form

$$\Psi(\mathbf{m}) = \Psi_{\mathrm{d}}(\mathbf{m}) + \alpha\, \Psi_{\mathrm{m}}(\mathbf{m}) \tag{5.14}$$

is sought to be minimized. Here,

$$\Psi_{\mathrm{d}}(\mathbf{m}) = \left\| \mathbf{W}_{\mathrm{d}} \left[\mathbf{d} - \mathbf{f}(\mathbf{m}) \right] \right\|^2 \tag{5.15}$$

is a measure of the data misfit, with **f** denoting the forward operator and $\mathbf{W}_{\mathrm{d}} = \mathrm{diag}(1/\varepsilon_1, ..., 1/\varepsilon_N)$ representing a data weighting matrix associated with the individual (uncorrelated) data errors ε_i. In addition, $\Psi(\mathbf{m})$ contains a stabilizing model objective function usually expressed as

$$\Psi_{\mathrm{m}}(\mathbf{m}) = \left\| \mathbf{W}_{\mathrm{m}} (\mathbf{m} - \mathbf{m}_{\mathrm{ref}}) \right\|^2, \tag{5.16}$$

which is used to incorporate certain model constraints relative to a reference model $\mathbf{m}_{\mathrm{ref}}$ by appropriate choice of a model weighting matrix $\mathbf{W}_{\mathrm{m}}$. The regularization parameter, α, in Equation (5.14) controls the tradeoff between influence of data misfit and model objective function in the inversion. Usually a smoothness constraint is imposed on the model, i.e., $\mathbf{W}_{\mathrm{m}}$ is chosen such as to evaluate the roughness of $\mathbf{m} - \mathbf{m}_{\mathrm{ref}}$. Using directional weights in the evaluation of model roughness, anisotropic smoothing may be applied (for example, Ellis and Oldenburg, 1994), for instance to account for a layered subsurface environment. The reference model $\mathbf{m}_{\mathrm{ref}}$ may contain expected parameter values as well as the result of a previous inversion in monitoring (time-lapse) applications, or just be assigned to a homogenous halfspace or the null vector if no additional information is available.

Minimization of Equation (5.14) can be achieved through application of gradient search methods. Adopting the Gauss-Newton approach, an iterative scheme results, where at each step, k, the linear system of equations

$$(\mathbf{J}_k^{\mathrm{T}} \mathbf{W}_{\mathrm{d}}^{\mathrm{T}} \mathbf{W}_{\mathrm{d}} \mathbf{J}_k + \alpha\, \mathbf{W}_{\mathrm{m}}^{\mathrm{T}} \mathbf{W}_{\mathrm{m}}) \Delta\mathbf{m}_k = \mathbf{J}_k^{\mathrm{T}} \mathbf{W}_{\mathrm{d}}^{\mathrm{T}} \mathbf{W}_{\mathrm{d}} [\mathbf{d} - \mathbf{f}(\mathbf{m}_k)] - \alpha\, \mathbf{W}_{\mathrm{m}}^{\mathrm{T}} \mathbf{W}_{\mathrm{m}} (\mathbf{m}_k - \mathbf{m}_{\mathrm{ref}}) \tag{5.17}$$

is solved for a model update $\Delta\mathbf{m}_k$. Here, $\mathbf{J}_k$ is the Jacobian (sensitivity) matrix; that is, $J_{ij} = \partial d_i / \partial m_j$, evaluated for the current model $\mathbf{m}_k$. Starting from a model $\mathbf{m}_0$ (for instance, homogenous or equal to $\mathbf{m}_{\mathrm{ref}}$, if available), the iteration process $\mathbf{m}_{k+1} = \mathbf{m}_k + \Delta\mathbf{m}_k$ according to Equation (5.17) is continued for an optimum choice of α (see for example,

deGroot-Hedlin and Constable, 1990) until $\Psi_d(\mathbf{m}_k)$ matches the desired data misfit target value.

Numerous dc resistivity inversion schemes have been proposed that are, apart from implementation details, in principle based on the above approach, including 2D and 3D approaches for both surface (for example, Loke and Barker, 1995) and cross-borehole (for example, LaBrecque et al., 1996) data. For the interpretation of time-lapse data, the scheme may be slightly modified to directly invert temporal changes in the data for relative model variations (Daily et al., 1992; LaBrecque and Yang, 2000; Kemna et al., 2002). Importantly, the approach can be also straightforwardly extended to include IP data in the inversion process, either in terms of time-domain chargeability according to Equation (5.10) (LaBrecque, 1991; Oldenburg and Li, 1994) or in terms of frequency-domain phase angle according to Equation (5.11) (Kemna and Binley, 1996; Kemna et al., 2000).

5.4.4 MODEL APPRAISAL

In order to reliably interpret resistivity or IP inversion results, some knowledge about the final model resolution is often desired. Generally, model resolution is a complicated function of numerous factors including electrode layout, measurement scheme, data signal-to-noise ratio, resistivity distribution, as well as parameterization and regularization used in the inversion. According to inverse theory (for example, Menke, 1989), the model resolution matrix

$$\mathbf{R} = (\mathbf{J}_k^T \mathbf{W}_d^T \mathbf{W}_d \mathbf{J}_k + \alpha \mathbf{W}_m^T \mathbf{W}_m)^{-1} \mathbf{J}_k^T \mathbf{W}_d^T \mathbf{W}_d \mathbf{J}_k \tag{5.18}$$

may be computed for the final inversion iteration k to assess how individual parameters are resolved in multidimensional imaging approaches. $\mathbf{R}$ may be defined as

$$\mathbf{m} = \mathbf{R}\mathbf{m}_{true}, \tag{5.19}$$

where $\mathbf{m}$ is the vector of parameters obtained by the inversion and $\mathbf{m}_{true}$ is the vector of true (unknown) parameters. Any deviations of $\mathbf{R}$ from the identity matrix indicate that inverted parameter values result from an averaging process in the inversion. Off-diagonal entries in $\mathbf{R}$ may be used to display the effect of regularization (for instance smoothing) on each parameter (for example, Alumbaugh and Newman, 2000). Use of only the diagonal of $\mathbf{R}$ has been shown to be insightful for image appraisal in cross-borehole applications (Ramirez et al., 1995).

Since the actual calculation of $\mathbf{R}$ in large-scale inverse problems is cumbersome, an indirect approach based on a simple accumulated sensitivity map, $\mathbf{s}$, according to (Park and Van, 1991; Kemna, 2000)

$$s_j = (\mathbf{J}_k^T \mathbf{W}_d^T \mathbf{W}_d \mathbf{J}_k)_{jj} \tag{5.19}$$

may be used as a computationally inexpensive alternative for image appraisal. Obviously, resolution is supposed to be low in model regions where sensitivity of the measurements is poor (i.e., $\mathbf{s}$ shows low values) and correspondingly regularization is more influential. Figure 5.14 shows a comparison of the two approaches, Equations (5.18) and (5.19), for the 2D cross-borehole example in Figure 5.11. Both images in Figure 5.14 illustrate the decrease in sensitivity away from the boreholes. In

addition, the resolution matrix in Figure 5.14a shows clearly the asymmetry in the image sensitivity caused by the distribution of resistivity. Any application that requires accurate estimation of electrical properties away from the boreholes must take into account the rapidly decreasing sensitivity. Imaging a tracer plume, for example, will result in an effective mass-balance error or, if the boreholes are spaced too far apart, no sensitivity to the change in pore fluid concentration.

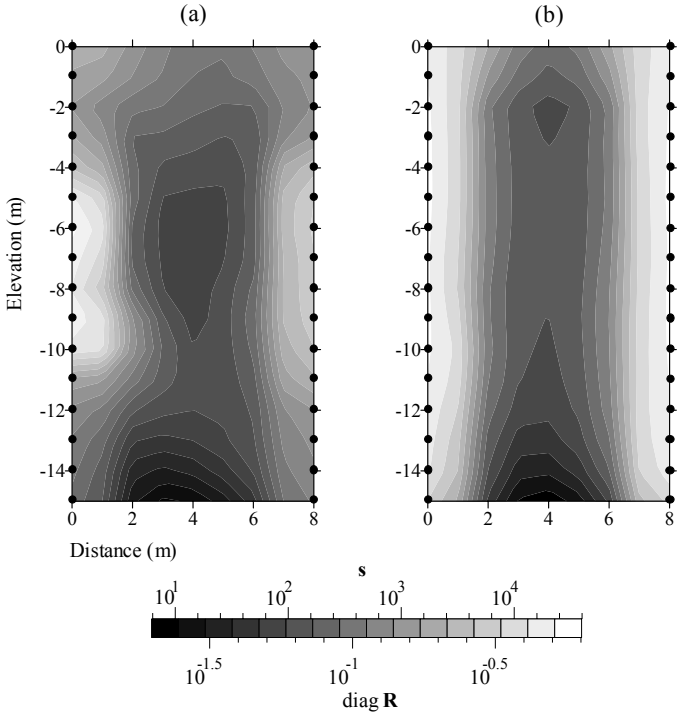

Figure 5.14. Illustration of resolution estimation for the 2D cross-borehole survey in Figure 5.11 (dark areas in images indicate poor resolution): (a) Diagonal of resolution matrix R in Equation (5.18), and (b) sensitivity map according to Equation (5.19). Note that (b) exhibits similar characteristics as (a).

An alternative procedure for assessing image resolution was proposed by Oldenburg and Li (1999). In their approach, two independent inversions for different reference models, $\mathbf{m}_{\text{ref}}^{(1)}$ and $\mathbf{m}_{\text{ref}}^{(2)}$, are computed, and the deviation of the respective inversion results, $\mathbf{m}^{(1)}$ and $\mathbf{m}^{(2)}$, is assessed in terms of the so-called depth of investigation index:

$$DOI_j = \frac{m_j^{(1)} - m_j^{(2)}}{m_{\text{ref}\,j}^{(1)} - m_{\text{ref}\,j}^{(2)}}. \tag{5.20}$$

In areas of the image where sensitivity is low, the *DOI* index will be close to unity, revealing regions where the model is weakly constrained by the data. Similarly, low *DOI* values will indicate high sensitivity and consequently allow greater faith in inverted values.

All of these model appraisal techniques are useful in assessing the uncertainty in areas of any image produced by an inverse method. These methods should be used, along with other factors discussed in the next section, to design an appropriate survey.

5.5. Survey design and implementation

For any investigation, the most appropriate survey configuration (surface, cross-borehole, etc.) will strongly depend on the specific objectives of the project. Surface arrays allow relatively rapid surveys to be carried out in a noninvasive manner, but depth of sensitivity will be limited. Galvanic contact is required for the electrodes, and consequently in some environments surface cover may limit the use of surface surveys. Investigations under areas where electrodes cannot be installed (under a building, for example) will also pose difficulties. In such environments, borehole arrays may prove more effective. However, the spacing between boreholes used for cross-borehole surveys should ideally be less than half the shortest length of an electrode array in any of the boreholes (as illustrated earlier).

The use of boreholes for electrode sites will often depend on the availability of existing boreholes or drilling budgets. Below the water table, electrodes can be lowered into open boreholes or slotted cased (non-metallic) boreholes. For vadose zone investigations, the electrodes will need to be sacrificially installed with an appropriate backfill to ensure good contact with the host material. For IP surveys, the backfill may significantly affect the measured polarization, and thus an appropriate backfill material must be selected. Bentonite, which is widely used for sealing sections of borehole backfill, will create significant polarization, which, even for dc resistivity, will cause problems in data quality.

The adopted measurement scheme (for example, Wenner, dipole-dipole, etc., for surface arrays) should be selected based on the expected target, but will also depend on environmental conditions and instrument availability. Dipole-dipole surveys, for example, are ideal for resolving localized targets (such as a tracer plume), but suffer from poor signal-to-noise ratios. Thus, high input voltages are required for dipole pairs that are widely spaced. For closely spaced dipoles, high voltage input will often result in “over voltages” (saturation of the receiver), and thus the dynamic range of the instrument needs to be considered before carrying out the survey. For surface dc resistivity surveys, the Wenner array is popular because of the good signal-to-noise ratio and reasonably narrow range of resistances measured in a typical survey. These factors allow the use of relatively inexpensive field instruments. In addition, a Wenner survey will enhance horizontal structures in the final image. While these may be appealing in many cases and give an indication of realism, in cases where the resistivity contrast is not horizontally layered, the Wenner array may be inappropriate. Ideally, synthetic model studies should be carried out before any survey to design the most appropriate configuration. Forward models are useful for computing the expected signals; these can be compared with the instrument resolution to assess the likely signal resolution. Inverse models, applied to synthetic targets, will allow the user to determine the expected resolution. Model appraisal methods, such as those discussed earlier, will

enhance the user's assessment of the appropriateness of the survey configuration selected.

To illustrate the use of synthetic studies, Figure 5.15 shows the results from three inverse models applied to a synthetic model representing a groundwater plume. The plume model is shown in Figure 5.15a. In Figure 5.15b the inversion of surface electrode data using a dipole-dipole scheme is shown. The target is reasonably well resolved, but is improved by using a reduced set of surface electrodes, combined with two widely spaced boreholes, as shown in Figure 5.15c. Using three boreholes, one of which intercepts the plume, results in a vast improvement in plume delineation, as shown in Figure 5.15d. In all these models a dipole-dipole scheme was used, and 2 % Gaussian noise was added to the forward model response prior to inversion. In addition, all forward model "measurements" with a transfer resistance lower than 10^{-3} ohm were ignored in the inversion to simulate instrument resolution.

For many hydrogeophysical studies of dynamic processes, the measurement scheme used will be constrained by data collection speed and the rate at which changes occur in the subsurface. Slow instrument relay switching results in data collection rates of two to four hundred measurements per hour. Many modern instruments offer multi-measurement channel capability, but each measurement "frame" may still take several hours for 3D configurations. Data collection speed should therefore also be recognized at the planning stage of any investigation.

If inverse methods are used, as is the case in many electrical surveys, the user should be aware of what is a satisfactory misfit between the model prediction and the data. This will depend on the error level in the data; however, for many resistivity surveys, users often fail to recognize the significance of data error in any investigation. Measurement errors in conventional surface resistivity surveys are traditionally assessed using repeatability checks. Such checks prove to be unreliable, particularly for cross-borehole surveys, and measurements of reciprocity are far superior in assessing true error levels. A reciprocity check is made by interchanging the electrode pair used for voltage measurement with the electrode pair used for current injection. The transfer impedance for these two cases will be identical if the system is responding linearly (i.e., according to Ohm's law) and there is no measurement error. Data errors should be used to weight the data (see Equation (5.15)). Over-fitting in data inversion results in "noisy" images and artifacts, which can be avoided by appropriate attention during data collection (see for example, LaBrecque et al., 1996).

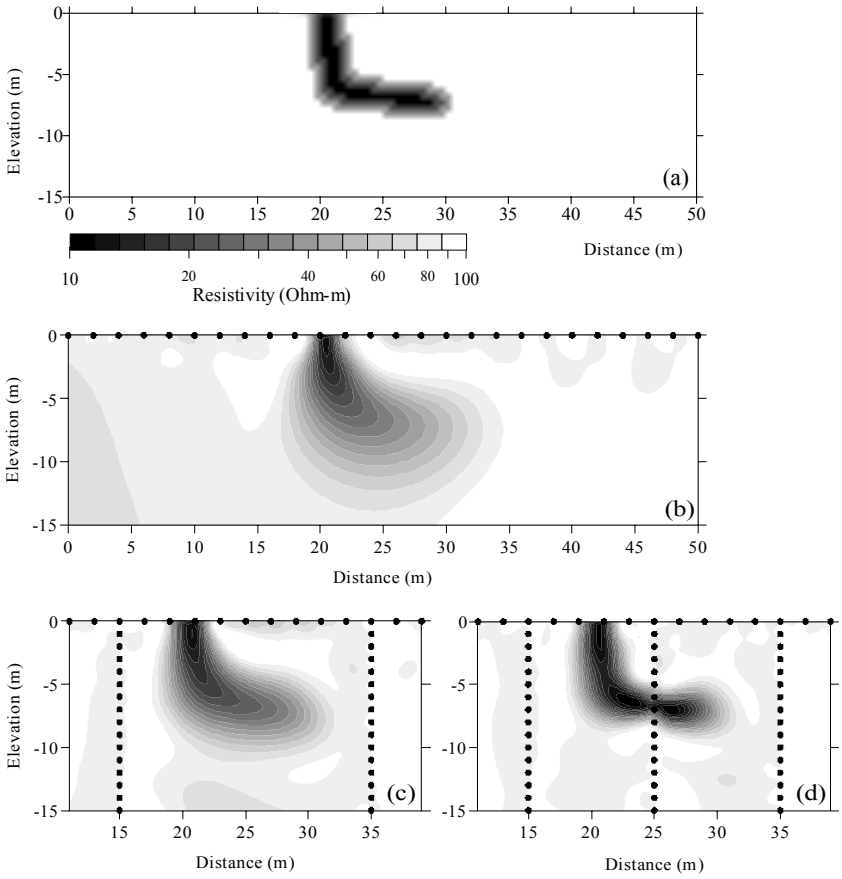

Figure 5.15. Synthetic plume model application: (a) synthetic model resistivity, (b) inverted model using only surface electrodes, (c) inverted model using surface electrodes and two borehole arrays, (d) inverted model using surface electrodes and three borehole arrays

The survey selected will also be influenced by the assumed spatial distribution of the electrical properties. Soundings are clearly not appropriate if significant 2D or 3D variability exists. Similarly, 2D (surface or cross-borehole) surveys may suffer from 3D effects; for cross-borehole surveys, these 3D effects may be result of the boreholes, or the backfill.

In summary, the hydrogeophysicist should consider a wide range of issues in selecting an appropriate survey. When appropriate, models should be used to ensure optimal subsurface characterization, and particular attention should be addressed to data quality prior to using any inverse method.

5.6. Future challenges

Despite their long history, electrical methods are still developing, yet many hydrogeophysical applications are currently constrained by the availability of appropriate hardware and software tools. Data collection speed is improving, but still remains a serious constraint for time-lapse 3D investigations. Autonomous data acquisition systems are emerging and offer great potential for remote monitoring of dynamic processes. Recently, Daily et al. (2004) demonstrated the use of such a system for remote monitoring of leakage from an underground storage tank.

Many inverse methods are based on a general smoothness constraint (see Equation (5.16)). However, for some cases assumptions of smoothness are not appropriate: sharp contrasts in the subsurface may exist, for example, at the edges of a contaminant or tracer plume or a lithological boundary. Alternative regularization approaches are being developed to address this problem (for example, Loke et al., 2001), and these offer promise for some future hydrogeophysical applications.

Linking electrical properties derived from electrical images to hydrological parameters, through relationships such as those covered in Chapter 4 of this volume, may permit estimation of hydraulic variables such as water content (for field examples, see Chapter 14 of this volume) or solute concentration (see for example, Kemna et al., 2002). Recently, Kemna et al. (2004b) proved in a synthetic experiment that time-lapse electrical imaging in conjunction with equivalent transport model analysis can actually be used to characterize solute transport in a heterogeneous aquifer in a quantitative manner. However, the effects of reduced sensitivity with distance from electrodes, coupled with smoothing effects from common regularization methods, will lead to poor mass balance. This limits the amount of quantitative information available to the hydrologist directly from an image. New approaches are needed that constrain image reconstruction, for instance based on the incorporation of flow models, such as proposed by Seppänen et al. (2001) for state estimation in process tomography, or by the incorporation of hydrologic-electrical parameter models (Liu and Yeh, 2004). The computation of geostatistical characteristics from electrical images is also likely to be an area of future research in hydrogeophysics, as such information can be of immense value to hydrological modelers. Joint hydraulic-geophysical inversion methods are also likely to develop. Dam and Christensen (2003) illustrate how hydraulic head and resistivity data may be used jointly to constrain groundwater model calibration, albeit through (perhaps limiting) assumptions of a relationship between hydraulic and electrical conductivity.

With rapidly developing hardware and software, some of which will be guided by hydrogeophysicists, we expect that there will be an increasing number of appropriate applications of electrical methods to an increasing range of hydrological problems, as well as greater integration of electrically derived information within hydrological modeling studies.

Acknowledgments

We would like to acknowledge the help of Lee Slater and Niels Christensen, whose excellent reviews greatly improved this chapter.

5.7. References

Alumbaugh, D.L., and G.A. Newman, Image appraisal for 2-D and 3-D electromagnetic inversion, *Geophysics*, *65*, 1455–1467, 2000.

Anderson, W.L., Numerical integration of related Hankel transforms of orders 0 and 1 by adaptive digital filtering, *Geophysics*, *44*, 1287–1305, 1979.

Barker, R.D., Signal contributions and their use in resistivity studies, *Geophys. J. Royal Astr. Soc.*, *59*, 123–129, 1979.

Bernard, J., and P. Valla, Groundwater exploration in fissured media with electrical and VLF methods, *Geoexploration*, *27*, 81–91, 1991.

Bevc, D., and H.F. Morrison, Borehole-to-surface electrical resistivity monitoring of a salt water injection experiment, *Geophysics*, *56*, 769–777, 1991.

Bing, Z., and S.A. Greenhalgh, Cross-hole resistivity tomography using different electrode configurations, *Geophys. Prosp.*, *48*, 887–912, 2000.

Bing, Z., and S.A. Greenhalgh, Finite element three-dimensional direct current resistivity modelling: Accuracy and efficiency considerations, *Geophys. J. Internat.*, *145*, 679–688, 2001.

Binley, A., S. Henry-Poulter, and B. Shaw, Examination of solute transport in an undisturbed soil column using electrical resistance tomography, *Water Resour. Res.*, *32*, 763–769, 1996.

Binley, A., P. Winship, L.J. West, M. Pokar, and R. Middleton, Seasonal variation of moisture content in unsaturated sandstone inferred from borehole radar and resistivity profiles, *J. Hydrol.*, *267*, 160–172, 2002a.

Binley, A., G. Cassiani, R. Middleton, and P. Winship, Vadose zone model parameterisation using cross-borehole radar and resistivity imaging, *J. Hydrol.*, *267*, 147–159, 2002b.

Börner, F.D., J.R. Schopper, and A. Weller, Evaluation of transport and storage properties in the soil and groundwater zone from induced polarization measurements, *Geophy. Prosp.*, *44*, 583–601, 1996.

Christensen, N.B., Optimized fast Hankel transform filters, *Geophys. Prosp.*, *27,* 876–901, 1990.

Christensen, N.B., and K. Sørensen, Pulled array continuous electrical sounding with an additional inductive source: An experimental design study, *Geophys. Prosp.*, *49*, 241–254, 2001.

Coggon, J.H., Electromagnetic and electrical modeling by the finite element method, *Geophysics*, *36*, 132–155, 1971.

Dahlin, T., On the automation of 2D resistivity surveying for engineering and environmental applications, PhD Thesis, Lund Univ., Sweden, 1993.

Dahlin, T., and M.H. Loke, Quasi-3D resistivity imaging-mapping of three-dimensional structures using 2D resistivity techniques, *Proc. 3rd Mtg. Environmental and*

Engineering Geophysics, Environ. Eng. Geophys. Soc., Eur. Section, 143–146, 1997.

Dahlin, T., V. Leroux, and J. Nissen, Measuring techniques in induced polarisation imaging, *J. Appl. Geophys.*, *50*, 279–298, 2002.

Dam, D., and S. Christensen, Including geophysical data in ground water model calibration, *Ground Water, 41*, 178–189, 2003.

Daily, W., and E. Owen, Cross borehole resistivity tomography, *Geophysics*, *56*, 1228–1235, 1991.

Daily, W.D., W. Lin, and T. Buscheck, Hydrological properties of Topopah Spring tuff: Laboratory measurements, *J. Geophys. Res.*, *92*, 7854–7864, 1987.

Daily, W.D., A.L. Ramirez, D.J. LaBrecque, and J. Nitao, Electrical resistivity tomography of vadose water movement, *Water Resour. Res*., *28*, 1429–1442, 1992.

Daily, W., A. Ramirez, and A. Binley, Remote monitoring of leaks in storage tanks using electrical resistance tomography: Application at the Hanford Site, *J. Environ. Eng. Geophys.*, *9*, 11–24, 2004.

deGroot-Hedlin, C., and S.C. Constable, Occam's inversion to generate smooth, two-dimensional models from magnetotelluric data, *Geophysics*, *55*, 1613–1624, 1990.

Dey, A., and H.F. Morrison, Resistivity modeling for arbitrarily shaped three-dimensional structures, *Geophysics*, *44*, 753–780, 1979a.

Dey, A., and H.F. Morrison, Resistivity modelling for arbitrarily shaped two-dimensional structures, *Geophys. Prosp.*, *27*, 106–136, 1979b.

Ellis, R.G., and D.W. Oldenburg, Applied geophysical inversion, *Geophys. J. Internat.*, *116*, 5–11, 1994.

French, H.K., C. Hardbattle, A. Binley, P. Winship, and L. Jakobsen, Monitoring snowmelt induced unsaturated flow and transport using electrical resistivity tomography, *J. Hydrol*., *267*, 273–284*,* 2002.

Frohlich, R.K., and C.D. Parke, The electrical resistivity of the vadose zone—Field survey, *Ground Water*, *27*, 524–530, 1989.

Hohmann, G.W., Numerical modeling for electromagnetic methods of geophysics, in *Electromagnetic Methods in Applied Geophysics, Vol. 1*, *Theory*, M.N. Nabighian, ed., Soc. Expl. Geophys., pp. 313–363, 1988.

Kalinski, R.J., W.E. Kelly, I. Bogardi, and I. Pesti, Electrical resistivity measurements to estimate travel times through unsaturated ground water protective layers, *J. Appl. Geophys.*, *30*, 161–173, 1993.

Kean, W.F., M.J. Waller, and H.R. Layson, Monitoring moisture migration in the vadose zone with resistivity, *Ground Water*, *27*, 562–571, 1987.

Kemna, A., Tomographic inversion of complex resistivity—Theory and application, PhD Thesis, Bochum Ruhr-Univ., Germany (published by: Der Andere Verlag, Osnabrück, Germany), 2000.

Kemna, A., and A. Binley, Complex electrical resistivity tomography for contaminant plume delineation, *Proc. 2nd Mtg. Environmental and Engineering Geophysics*, Environ. Eng. Geophys. Soc., Eur. Section, 196–199, 1996.

Kemna, A., A. Binley, A.L. Ramirez, and W.D. Daily, Complex resistivity tomography for environmental applications, *Chem. Eng. J.*, *77*, 11–18, 2000.

Kemna, A., J. Vanderborght, B. Kulessa, and H. Vereecken, Imaging and characterisation of subsurface solute transport using electrical resistivity

tomography (ERT) and equivalent transport models, *J. Hydrol.*, *267*, 125–146, 2002.

Kemna, A., A. Binley, and L. Slater, Cross-borehole IP imaging for engineering and environmental applications, *Geophysics*, *69*, 97–107, 2004a.

Kemna, A., J. Vanderborght, H. Hardelauf, and H. Vereecken, Quantitative imaging of 3D solute transport using 2D time-lapse ERT: A synthetic feasibility study, *Proc. Symp. Application of Geophysics to Engineering and Environmental Problems*, Environ. Eng. Geophys. Soc., 342-353, 2004b.

Koefoed, O., 1979, *Geosounding Principles, Vol. 1: Resistivity Sounding Measurements*, Elsevier Science Publ. Co., Inc., 1979.

Kosinski, W.K., and W.E. Kelly, Geoelectric soundings for predicting aquifer properties, *Ground Water*, *19*, 163–171, 1981.

LaBrecque, D.J., IP tomography, *61st Ann. Internat. Mtg.*, *Expanded Abstracts*, Soc. Expl. Geophys., 413–416, 1991.

LaBrecque, D.J., M. Miletto, W. Daily, A. Ramirez, and E. Owen, The effects of noise on Occam's inversion of resistivity tomography data, *Geophysics*, *61*, 538–548, 1996.

LaBrecque, D.J., and X. Yang, Difference inversion of ERT data: A fast inversion method for 3-D in-situ monitoring, *Proc. Symp. Application of Geophysics to Engineering and Environmental Problems*, Environ. Eng. Geophys. Soc., 723–732, 2002.

Li, Y., and K. Spitzer, Three-dimensional dc resistivity forward modelling using finite elements in comparison with finite-difference solutions, *Geophys. J. Internat.*, *151*, 924–934, 2002.

Liu, S., and T.-C.J. Yeh, An integrative approach for monitoring water movement in the vadose zone, *Vadose Zone J.*, in press, 2004.

Loke, M.H., and R.D. Barker, Least-squares deconvolution of apparent resistivity pseudosections, *Geophysics*, *60*, 1682–1690, 1995.

Loke, M.H., and R.D. Barker, Practical techniques for 3D resistivity surveys and data inversion, *Geophys. Prosp.*, *44*, 499–523, 1996.

Loke, M.H, I. Acworth, and T. Dahlin, A comparison of smooth and blocky inversion methods in 2-D electrical imaging surveys, *Proc. 15th Geophysical Conference and Exhibition*, Austr. Soc. Expl. Geophys., 2001.

Lowry, T., M.B. Allen, and P.N. Shive, Singularity removal: A refinement of resistivity modeling techniques, *Geophysics*, *54*, 766–774, 1989.

Lytle, R.J., and K.A. Dines, An impedance camera: A system for determining the spatial variation of electrical conductivity, *Lawrence Livermore National Laboratory Report UCRL-52413*, Livermore, California, USA, 1978.

Menke, W., *Geophysical Data Analysis: Discrete Inverse Theory*, Academic Press, Inc., 1989.

Mussett, A.E., and M.A. Khan, *Looking into the Earth. An Introduction to Geological Geophysics*, Cambridge University Press, 2000.

Nimmer, R.E., and J.L Osiensky, Direct current and self-potential monitoring of an evolving plume in partially saturtated fractured rock, *J. Hydrol.*, *267*, 258–272, 2001.

Oldenburg, D.W., and Y. Li, Inversion of induced polarization data, *Geophysics*, *59*, 1327–1341, 1994.

Oldenburg, D.W., and Y. Li, Estimating depth of investigation in dc resistivity and IP surveys, *Geophysics*, *64*, 403–416, 1999.

Osiensky, J.L., Ground water modeling of mise-a-la-masse delineation of contaminated ground water plumes, *J. Hydrol.*, *197*, 146–165, 1997.

Panissod, C., M. Lajarthe, and A. Tabbagh, Potential focusing: A new multielectrode array concept, simulation study and field tests in archaeological prospecting, *J. Appl. Geophys.*, *38*, 1–23, 1997.

Park, S.K., and G.P. Van, Inversion of pole-pole data for 3-D resistivity structure beneath arrays of electrodes, *Geophysic*s, *56*, 951–960, 1991.

Pridmore, D.F., G.W. Hohmann, S.H. Ward, and W.R. Sill, An investigation of finite-element modeling for electrical and electromagnetic data in three dimensions: *Geophysics*, *46*, 1009–1024, 1981.

Ramirez, A., and W. Daily, Electrical imaging at the large block test—Yucca Mountain, Nevada, *J. Appl. Geophys.*, *46*, 85–100, 2001.

Ramirez, A., W. Daily, D. LaBrecque, E. Owen, and D. Chesnut, Monitoring an underground steam injection process using electrical resistance tomography, *Water Resour. Res.*, *29*, 73–87, 1993.

Ramirez, A., W.D. Daily, and R.L. Newmark, Electrical resistance tomography for steam injection monitoring and process control, *J. Environ. Eng. Geophys*., *0*, 39–51, 1995.

Ramirez, A., W. Daily, A. Binley, D. LaBrecque, and D. Roelant, Detection of leaks in underground storage tanks using electrical resistance methods, *J. Environ. Eng. Geophys*., *1*, 189–203, 1996.

Reynolds, J.M., *An Introduction to Applied and Environmental Geophysics*, Wiley, 1998.

Seigel, H.O., Mathematical formulation and type curves for induced polarization, *Geophysic*s, *24*, 547–565, 1959.

Schima, S., D.J. LaBrecque, P.D. Lundegard, Using resistivity tomography to monitor air sparging, *Ground Water Monitoring and Remediation*, *16*, 131–138, 1996.

Schenkel, C.J., Resistivity imaging using a steel cased well, *Lawrence Livermore National Laboratory Report UCRL-JC-121653*, Livermore, California, USA, 1995.

Seppänen, A., M. Vauhkonen, P.J. Vauhkonen, E. Somersalo, and J.P. Kaipio, State estimation with fluid dynamical evolution models in process tomography: An application to impedance tomography, *Inverse Problems*, *17*, 467-483, 2001.

Simms, J.E. and F.D. Morgan, Comparison of four least-squares inversion schemes for studying equivalence in one-dimensional resistivity interpretation, *Geophysics*, *57*, 1282–1293, 1992.

Slater, L., and D. Lesmes, IP interpretation in environmental investigations, *Geophysics*, *67*, 77–88, 2002.

Slater, L., A. Binley, W. Daily, and R. Johnson, Cross-hole electrical imaging of a controlled saline tracer injection, *J. Appl. Geophys.*, *44*, 85–102, 2000.

Sørensen, K., Pulled array continuous electrical profiling, *First Break*, *14*, 85–90, 1996.

Spitzer, K., A 3-D finite-difference algorithm for dc resistivity modelling using conjugate gradient methods, *Geophys. J. Internat*., *123*, 903–914, 1995.

Taylor, R.W., and A.H. Fleming, Characterizing jointed systems by azimuthal resistivity surveys, *Ground Water*, *26*, 1988.

Telford, W.M., L.P. Geldart, and R.E. Sheriff, *Applied Geophysics*, 2nd ed., Cambridge Univ. Press, 1990.

Tikhonov, A.N., and V.Y. Arsenin, *Solutions of Ill-Posed Problems*, W.H. Winston and Sons, 1977.

Weller, A., M. Seichter, and A. Kampke, Induced-polarization modelling using complex electrical conductivities, *Geophys. J. Internat*., *127*, 387–398, 1996.